高レイノルズ数壁乱流における微粒子の加速度統計に関する研究: 大きな圧力変動に起因する乱流構造の抽出

課題責任者
辻　　義之　　名古屋大学大学院工学研究科

著者
山本　義暢*[1]，　恒吉　達矢*[2]，Ali Mehrez*[2]
[1]山梨大学工学部，[2]名古屋大学大学院工学研究科

せん断乱流中の流体粒子加速度の統計的性質を調べるために，チャネル乱流の直接数値計算(DNS)をおこなった．流体粒子加速度は，せん断乱流の壁近くでは，乱流渦構造の影響を大きく受ける．壁面圧力での条件付け平均の結果から，正の圧力変動は速度せん断層，負の圧力変動は微細渦構造に関連することが明らかになった．また，正負の高圧領域はヘアピン型の渦構造と密接に関連しており，渦構造は壁からの距離に対して自己相似的に存在する可能性が明らかになった．

キーワード：粒子加速度，乱流渦構造，壁面圧力，せん断流れ，間欠性

1. はじめに

せん断乱流中の流体粒子加速度の統計的性質を調べるために，チャネル乱流の直接数値計算(DNS)をおこなった[1]．流体粒子加速度は，せん断乱流の壁近くでは，乱流渦構造の影響を大きく受けることが予想される．乱流渦構造は，内部で負の絶対値の大きな圧力（HAPPK: High Amplitude Pressure Peak）を示すため，壁面での圧力変動から渦構造を抽出できるかを明らかにし，また，乱流渦構造の Re 数に対する変化について，そのスケーリングを昨年度報告した．

本年度は，圧力変動の分散$\langle p^{+2}\rangle$が壁からの距離に対して対数的に変化する要因を乱流構造との関連で調べる．変動圧力のみならず，スパン方向の変動強度$\langle w^{+2}\rangle$についても同様に対数分布が確認されるが，その物理的根拠を DNS データを用いて明らかにする．

壁面圧力の HAPPK による条件付き平均から，ヘアピン型の渦構造を抽出できた．正の高圧力領域はヘアピン渦が壁面に接する両足の間に確認され，負の高圧領域は渦のヘアピン部（上部）に存在する．正負の高圧領域は密接に渦構造と関連しており[2,3]，渦構造が壁からの距離に対して自己相似的に存在しうることが分かった[4]．

2. 数値計算手法

解析対象は，一定の圧力勾配で駆動される 2 次元チャンネル乱流場である．図１に解析領域を示す．xを主流方向，yを壁垂直方向，zをスパン方向とする．基礎方程式は，非圧縮性流体のナビエ・ストークス方程式及び連続式とし，擬スペクトル法に基づき計算が行われている．離散化手法は，主流及びスパン方向にフーリエスペクトル法，壁垂直方向に 2 次精度の中心差分を使用し，主流及びスパン方向へのエイリアジング誤差は位相シフト法によりこれを除去してある．位相シフト法とはフーリエ空間上において位相を変化させた関数と本来の関数の和を取ることにより，エイリアジング誤差を除去する手法である．時間進行は，対流項に 3 次精度 Runge-Kutta 法，粘性項に Crank-Nicolson 法，圧力項に Euler 陰解法を使用し，境界条件は，主流及びスパン方向に周期境界条件，壁面で no-slip 条件を課してある．計算格子には直交格子を用いており，主流方向，スパン方向には等間隔に格子を配置している．壁垂直方向には壁面近傍における粘性の影響を考慮するために，壁近くにかけてメッシュを細かくしてある．計算条件は Re_τ=150，600，1000，2000，4000 である．各レイノルズ数における解析対象の x，y，z 方向の計算領域(L_x，L_y，L_z)，格子点数(N_x，N_y，N_z)を表 3-1 に示す[1]．

DNS データベースには速度 3 成分（主流方向速度，壁垂直方向速度，スパン方向速度）と圧力のデータが保存されている．各々の成分について 3 次元の空間データが時系列方向に保存されており，時間方向データ数を n_t とすると，data_1～data_n_t というディレクトリが存在している．また，時間番号を示すディレクトリ配下には壁垂直方向(y)の 2 次元平面(x, z)のデータが壁垂直方向の昇順に保存してある．

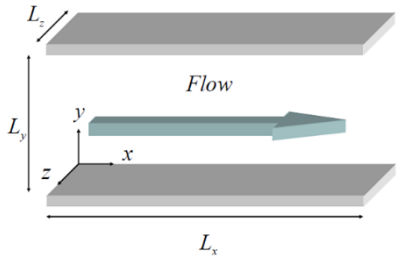

図１　計算対象のとなるチャネル乱流場

3. 結果及び考察

乱流構造を議論するために，変動圧力p とスパン方向変動速度wとの空間相関を定義しておく．変動値には，空間スケール$0.7h$よりも小さなスケールを抽出するために，空間フィルターをかけている[5]．

$$c_{\psi_s\psi_s}(\Delta x, y, \tilde{y}, \Delta z) = \frac{\langle \psi_s(X)\psi_s(\tilde{X})\rangle}{\psi_{rms}(y)\,\psi_{rms}(\tilde{y})}, \qquad (1)$$

ここで，ψ と ψ_s は，オリジナルな変動とフィルターをかけた小スケール変動をあらわし，$X=(x,\ y,\ z)$，$\Delta x = x-\tilde{x}$，$\Delta z = z-\tilde{z}$ とする．$\tilde{X}=(\tilde{x},\ \tilde{y},\ \tilde{z})$ は参照点であり，オリジナルは変動量の分散で無次元化してある．相関係数$c_{p_sp_s}$および$c_{w_sw_s}$分布を Fig. 1 に示す．正の相関は黒，負の相関は青色で示してある．相関係数の分布は，p とw に対して類似の分布を持つことがわかる．この傾向は Sillero *et al.* [6]によってもすでに議論されている．本結果から，$c_{p_sp_s}$ と $c_{w_sw_s}$ は同じ距離にわたって相関を持つが，流れ方向へは異なった角度で傾いており，p と wが乱流構造の異なる位置か反映していると考えられる．Fig. 1(d)にみられるように，スパン方向の速度相関には2つの負の相関領域（$c_{w_sw_s}=-0.05$）が確認できる．

圧力とスパン方向速度の小スケール変動の空間相関係数を以下に定義する．

$$c_{p_sw_s}(\Delta x, y, \tilde{y}, \Delta z) = \frac{\langle w_s(X)p_s(\tilde{X})\rangle}{w_{rms}(y)\,p_{rms}(\tilde{y})}, \qquad (2)$$

相関の分布を Fig. 2 に示した（$\tilde{y}/h \approx 0.1$ and $Re_\tau = 1000$）．正負の相関係数の分布は，ほぼ対称性を示しており，それらはスパン方向に広がっている．この結果は，p とw の間に共通の乱流構造が存在することを示唆しており，スパン方向には，反対の符号を持つ．さらに，Fig. 2(b)に示したわずかな相関 $c_{p_sw_s}=\pm 0.05$ は，壁に対して構造の傾きが異なることを表している．特に，Fig. 2(b)に示した正負の相関は，傾いた構造の傾向をよく表現しており、黒と青の等値線で示してある．

表１　直接数値計算の計算条件

Re_τ	$\frac{L_x}{h}$	$\frac{L_z}{h}$	Δx^+	Δz^+	Δy_w^+	Δy_c^+	N_y	$\frac{T^+}{Re_\tau}$
180	12.8	6.4	12.0	7.2	0.3	3.8	192	12.4
400	12.8	6.4	13.3	6.7	0.17	4.3	384	10.4
1000	12.8	6.4	13.3	8.3	0.6	8.0	512	11.2
2000	16.0	6.4	16.0	8.3	0.6	8.0	1024	8
4000	16.0	6.4	15.6	8.3	0.6	8.0	2048	8

4. まとめ

圧力変動の分散$\langle p^{+2}\rangle$が壁からの距離に対して対数的に変化する要因とスパン方向の変動強度$\langle w^{+2}\rangle$についても同様に対数分布が確認される，その物理的要因は共通の乱流構造に関連していることを明らかにした．小スケール変動の空間相関を調べることで，乱流強度の対数分布に寄与する構造は小スケール変動と考えられる．空間相関の分布から，乱流構造はヘアピン型の渦と予想される．正の相関は壁に接する脚の間に，負の相関は渦の頂部に存位する．スパン方向速度は，ヘアピン渦の足部分と頂部まわりに存在する．薄構造は，p と w の変動に強い相関をもたらす小スケールであり、それらは壁からの距離に対して相似的分布を示す．これらの渦構造は、壁近くでの流体粒子の大きな加速度変動と関連していることが予想される．さらに詳しく加速度統計との関係を調べていく必要がある[4]．

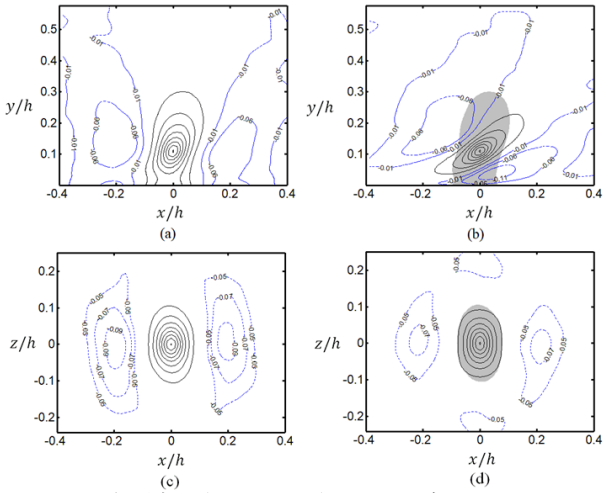

FIG. 1 参照点を$(\tilde{y}/h \approx 0.1)$とした場合の小スケールの空間相関係数 $c_{p_sp_s}$ の分布を(a, c)に示す．(b, d)にはスパン方向速度の相関係数$c_{w_sw_s}$を示す．正の相関は黒実線，負の相関は青色波線で示してあり，等値線の間隔は[0.1:0.1:0.7]とした．

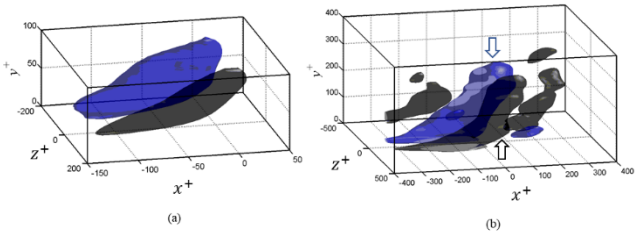

FIG. 2 参照点を$(\tilde{y}/h \approx 0.1)$とした場合の小スケールの空間相関係数 $c_{p_sp_s}$ の分布を三次元空間で示した．(a) $c_{p_sw_s}=\pm 0.08$ (b) $c_{p_sw_s}=\pm 0.03$である．正負の相関は，黒と青の等値面で示されている．

参考文献

[1] Yoshinobu Yamamoto and Yoshiyuki Tsuji, Numerical evidence of logarithmic regions in channel flow at Reτ=8000,Phys. Rev. Fluids 3, 012602(R) ,2018

[2] Johansson, A. V., Her, J. Y., and Haritonidis, J. H., 1987, “On The Generation of high-amplitude Wall-Pressure Peaks in Turbulent Boundary Layers and Spots”, *J. Fluid Mech.*, Vol. 175, pp. 119-142.

[3] Johansson, A. V., Alfredsson, P. H., and Kim, J., 1991, “Evolution and Dynamics of Shear-Layer Structures in Near-Wall Turbulence”, *J. Fluid Mech.*, Vol. 224, pp. 579-599.

[4] Ali Mehrez, Jimmy Philip, Yoshinobu Yamamoto, and Yoshiyuki Tsuji, Pressure and spanwise velocity fluctuations in turbulent channel flows: Logarithmic behavior of moments and coherent structures, Phys. Rev. Fluids 4, 044601(2019).

[5] J. Jiménez, Coherent structures in wall-bounded turbulence, J. Fluid Mech. 842, 1 (2018).

[6] J. A. Sillero, J. Jiménez, and R. D. Moser, Two-point statistics for turbulent boundary layers and channels at Reynolds numbers up to $\delta^+ \approx 2000$, Phys. Fluids 26, 105109 (2014).

Lagrange Acceleration of Small Particles in Wall Bounded Flow; High-amplitude Wall Pressure Events and Their Relation to Turbulent Structures in Channel Flow

Project Representative
Yoshiyuki Tsuji Graduate School of Engineering, Nagoya University

Authors
Yoshinobu Yamamoto*[1], Tatsuya Tsuneyoshi*[2], Ali Meherez*[2]
*[1]Department of Engineering, Yamanashi University, *[2]Graduate School of Engineering, Nagoya University

Direct Numerical simulation Data (DNS) set of fully developed turbulent channel flow is utilized to study the Lagrange acceleration of fluid particle in shear flow. Fluid particles may be strongly affected by the turbulent structures near the wall, and their structures indicate the negative high-amplitude pressure in the core region. Positive wall pressure is associated to the velocity shear layers.

Keywords：particle acceleration, turbulent eddy structures, wall pressure, shear layer, intermittency

1. Introduction

Direct Numerical simulation Data (DNS) set of fully developed turbulent channel flow is utilized to study the Lagrange acceleration of fluid particle in shear flow [1]. Fluid particles are strongly affected by the turbulent structures near the wall, and their structures indicate the negative high-amplitude pressure in the core region. In this report, the turbulent structures associated with positive and negative High Amplitude Pressure Peaks (HAPPKs) at different Reynolds number are studied[2,3].

We study the logarithmic behavior of the pressure variance $\langle p^{+2} \rangle$ from the datasets obtained from direct numerical simulations of turbulent channel flow for friction Reynolds number Re_τ up to 4000. The higher-order moments of p were found to follow logarithmic behaviors at the same distances from the wall where $\langle p^{+2} \rangle$ shows its log-profile. Same results have been confirmed for the spanwise velocity fluctuations w at the same Reynolds numbers, with both p and w following a super-Gaussian behavior. The minimum Reynolds number for $\langle p^{+2} \rangle$ and $\langle w^{+2} \rangle$ log-profiles to appear is $Re_\tau \approx 500$, where flow structures $\mathcal{O}(h)$ or less were found to significantly contribute to these profiles. The configuration of the hairpin eddy structures obtained from the conditional sampling at different wall-normal locations showed a strong link between p and w fluctuations. Positive pressure fluctuations are located between the legs of the hairpin eddy, while the negative pressure fluctuations are consistent with the head part of the hairpin eddy. Positive and negative spanwise velocity fluctuations are strongly positioned with the legs of the hairpin eddy, consistent with the counter-rotating motion resulting from the eddy legs. The structures were also found to be geometrically self-similar such that their length and their width increase linearly with the distance from the wall[4].

2. Numerical Simulation

The simulations reported in this study are DNSs of incompressible turbulent flow between two parallel planes. The coordinate system is taken to be (x, y, z) that are representing the streamwise, wall-normal, and spanwise coordinates, respectively with $u_i = (u_1, u_2, u_3) = (u, v, w), i = 1,2,3$ are the three components of velocity in the same directions. For the pressure, p is used to denote the total pressure. In streamwise (x) and spanwise (z) directions, periodic boundary conditions are applied, and no-slip/no-penetration boundary conditions are applied at the wall. The mass flux through the channel remains constant by a uniform streamwise pressure gradient that drives the flow field.

DNSs of the incompressible Navier–Stokes equation are conducted by a hybrid Fourier spectral (x, z) and the second-order central difference method in (y) direction, where aliasing error in the streamwise and spanwise directions is removed by the phase shift method. For time progress, third-order accuracy Runge-Kutta method is applied to the convection term, Crank-Nicolson method is applied to the viscosity term, and the Euler implicit method is applied to the pressure term. The present DNS conditions are shown in Table 1. The domain size is relatively large to detect the large-scale structures exist around the center of the channel. The time taken for a hypothesized turbulent eddy to perform one complete 360° rotation and, known as eddy turn over time T^+, is given also in Table 1.

Table 1. Calculation conditions for DNS data set

Re_τ	$\frac{L_x}{h}$	$\frac{L_z}{h}$	Δx^+	Δz^+	Δy_w^+	Δy_c^+	N_y	$\frac{T^+}{\mathrm{Re}_\tau}$
180	12.8	6.4	12.0	7.2	0.3	3.8	192	12.4
400	12.8	6.4	13.3	6.7	0.17	4.3	384	10.4
1000	12.8	6.4	13.3	8.3	0.6	8.0	512	11.2
2000	16.0	6.4	16.0	8.3	0.6	8.0	1024	8
4000	16.0	6.4	15.6	8.3	0.6	8.0	2048	8

Table 1 illustrates the computational domain size in streamwise and spanwise directions (L_x, L_z), in addition to the grid resolutions in the three directions $(\Delta x^+, \Delta y^+, \Delta z^+)$, where Δy_w^+ represents the grid resolution at the wall, and Δy_c^+ is at the center of the channel. Table 1 gives the number of grid points in N_y the wall-normal direction.

3. Results and Discussions

Before discussing the coherent structures in the next section and to further clarify the relation between p and w fields, we define the correlation function of the filtered pressure and spanwise velocity fluctuations. The autocorrelation function for the small-scale of p and w, following Jiménez [5], is defined as

$$c_{\psi_s\psi_s}(\Delta x, y, \tilde{y}, \Delta z) = \frac{\langle \psi_s(X)\psi_s(\tilde{X})\rangle}{\psi_{rms}(y)\,\psi_{rms}(\tilde{y})}, \qquad (1)$$

where ψ and ψ_s refer respectively to the total and small-scale of p and w (smaller than $0.7h$). Here, $X = (x, y, z)$, $\Delta x = x - \tilde{x}$, $\Delta z = z - \tilde{z}$, and $\tilde{X} = (\tilde{x}, \tilde{y}, \tilde{z})$ is the reference position. The local root mean square (r.m.s.) values of the total p and w are selected for the normalization. The correlation of the small-scale pressure $c_{p_sp_s}$ and spanwise velocity $c_{w_sw_s}$ are shown in Figs. 1(a) and (b), respectively, for $x-y$ sections, and for $x-z$ sections in Figs. 1(c) and (d). In each panel, positive and negative correlations are represented by the black and blue contours, respectively. In Figs. 1(b) and (d), the gray patches represent $c_{p_sp_s}$. They are displayed on the same plots of $c_{w_sw_s}$ for the purpose of comparison. The reference position is taken at $\tilde{y}/h \approx 0.1$ for $Re_\tau = 1000$. The correlations $c_{p_sp_s}$ and $c_{w_sw_s}$ show similar features observed for total p and w which were discussed in details by Sillero *et al.* [6]; however, here they are correlated at smaller length scales due to the filtering process. A significant point here is that both $c_{p_sp_s}$ and $c_{w_sw_s}$ are correlated over the same distances, which is apparent in Fig. 1(d) for the positive $c_{p_sp_s}$ and $c_{w_sw_s}$ in $x-z$ sections. For $x-y$ sections in Fig. 1(b), positive $c_{p_sp_s}$ and $c_{w_sw_s}$ also have the same length with different inclinations to the wall. This is because p and w fluctuations have different orientations with respect to their common structures. Another noteworthy point regarding Fig. 1(d) is that for the spanwise velocity fluctuations, there are two negative blobs ($c_{w_sw_s} = -0.05$) on two sides aligned along the spanwise direction. Interestingly, these two negative correlations are not indicated for the total w fluctuations discussed by Sillero *et al.* [6].

The cross-correlation function $c_{p_sw_s}$ of the small-scale pressure-spanwise velocity fluctuations is defined as

$$c_{p_sw_s}(\Delta x, y, \tilde{y}, \Delta z) = \frac{\langle w_s(X)p_s(\tilde{X})\rangle}{w_{rms}(y)\,p_{rms}(\tilde{y})}, \qquad (2)$$

and is shown in Fig. 2 for the same values of $\tilde{y}/h \approx 0.1$ and $Re_\tau = 1000$. The small-scale pressure is selected to be fixed at the reference position. For the value of the correlation $c_{p_sw_s} = \pm 0.08$ shown in Fig. 2(a), the positive and negative correlations are approximately symmetric, and they are aligned along the spanwise direction. This alignment indicates that the common structures between p and w fluctuations induce w fluctuations with opposite signs along z direction. Further, the weak correlations $c_{p_sw_s} = \pm 0.05$ depicted in Fig. 2(b) indicate that the correlations take different inclinations with respect to the wall (positive and negative correlations are highlighted by black and blue arrows in Fig. 2(b), respectively).

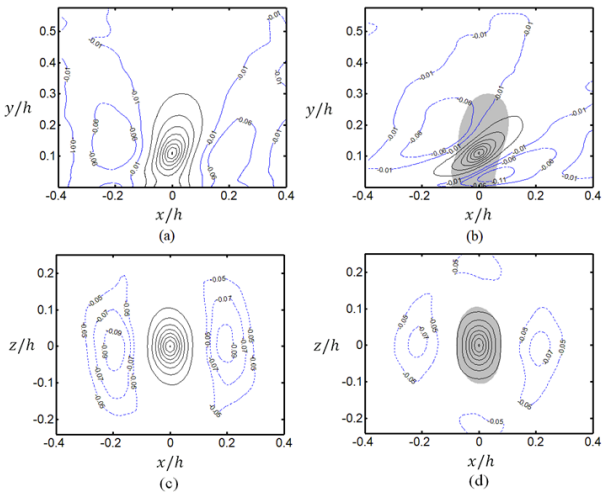

FIG. 1 Two-dimensional sections through the reference point $(\tilde{\boldsymbol{y}}/\boldsymbol{h} \approx \mathbf{0.1})$ of the two-point autocorrelation function of the small-scale (a, c) pressure $\boldsymbol{c_{p_sp_s}}$, and (b, d) spanwise velocity $\boldsymbol{c_{w_sw_s}}$ at $\boldsymbol{Re_\tau = 1000}$. $\boldsymbol{x-y}$ sections are represented in (a) and (b) for $\boldsymbol{c_{p_sp_s}}$ and $\boldsymbol{c_{w_sw_s}}$, respectively. $\boldsymbol{x-z}$ sections are introduced in (c) and (d) for $\boldsymbol{c_{p_sp_s}}$ and $\boldsymbol{c_{w_sw_s}}$, respectively. Positive correlations are indicated by the black color with values $[\mathbf{0.1}:\mathbf{0.1}:\mathbf{0.7}]$, while the blue dashed contours represent negative correlations. In (b) and (d), the gray patches represent $\boldsymbol{c_{p_sp_s}}$.

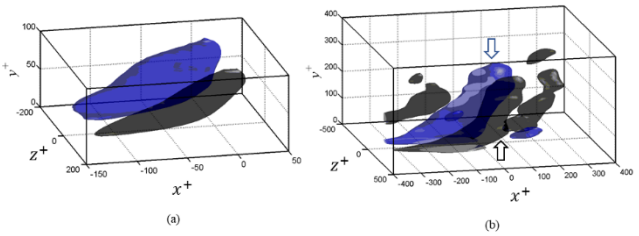

FIG. 2 Three-dimensional view of the cross-correlation function $c_{p_sw_s}$ of the small-scale pressure-spanwise velocity fluctuations at the reference point $(\tilde{y}/h \approx 0.1)$ for $Re_\tau = 1000$. In (a), $c_{p_sw_s} = \pm 0.08$ and in (b), $c_{p_sw_s} = \pm 0.03$. Positive and negative correlations are represented by the black and the blue colors, respectively.

The common structure between p and w fluctuations that could be inferred from the cross-correlation function is the hairpin-type eddy. The legs and the neck of the hairpin eddy are consistent with the different inclinations of the positive and negative correlations. The hairpin eddy configuration was not suggested by Sillero *et al.* [6] and Jiménez [5]. They

recommended the structure associated with w fluctuations to be a quasi-streamwise roller that scales in outer units. Note that quasi-streamwise rollers were obtained from the correlations of the total w and v fluctuations. Upon computing the correlation length of the pressure fluctuations, Jiménez [5] also stated that these rollers are the dominant structures for the pressure fluctuations. Here, we are concerned with the small-scale of motions for p and w fluctuations that show a common log-profile, and these correlations suggest a configuration of the hairpin kind. Besides, the autocorrelation functions $c_{p_s p_s}$ and $c_{w_s w_s}$ presented in Fig. 1 are correlated over the same distances.

4.Summary

The pressure variance starts its logarithmic profiles at wall-normal location of approximately 150 in wall units, while the log-profile of the spanwise velocity variance starts closer to the wall at around 90 in wall units, independent of Reynolds number. The upper bounds of both profiles show linear relations with Re_τ with the same slope of around 0.2. The log-regions of $\langle p^{+^2} \rangle$ and $\langle w^{+^2} \rangle$ overlap each other over significantportions of the wall-distance, and the minimum Reynolds number estimated for both log-regions to be identified is $Re_\tau \approx 500$. Besides, we have studied the higher-order moments of p and w, where the $2n-$order moments raised to the power of $1/n$, with $n = 1, \ldots, 4$, follow the logarithmic behaviors within the same regions where $\langle p^{+^2} \rangle$ and $\langle w^{+^2} \rangle$ confirm the log-profiles. In addition, the higher-order moments of p and w follow super-Gaussian behaviors which reinforce the similarity between p and w. The implication of the logarithmic scaling of the higher-order moments of p and w fluctuations is their association with a hierarchical organization of self-similar eddies.

The coherent structures related to the pressure intensity log-profile, and hence and the spanwise velocity, are also investigated. The instantaneous fields of p and w are decomposed into small- and large-scales of motion with sharp spectral filters $\lambda_{xc} = \lambda_{zc} = 0.7h$ which are associated with the ridge of the spectra at the upper bound of $\langle w^{+^2} \rangle$ log-profile. The small-scales of motion showed that they are the main contributors to the log-trends of p and w. We used the conditional sampling technique to explore the structures associated with these small-scales of motion. The conditional sampling around the positive high-amplitude small-scale pressure fluctuations at different wall-normal locations results in hairpin eddy structures. Positive pressure fluctuations are located between the legs of the hairpin eddy, while the negative pressure fluctuations are consistent with the head part of the hairpin eddy. Positive and negative spanwise velocity fluctuations are strongly positioned consistently with the legs and neck of the hairpin eddy. The eddy structure shows a strong link between p and w fluctuations, both of which occur at relatively smaller scales. Furthermore, these small-scale structures are found to be geometrically self-similar. Their length and width increase linearly with the distance from the wall. As such, the size of the eddy does not change when it is scaled with the distance from the wall.

REFEENCS

[1] Yoshinobu Yamamoto and Yoshiyuki Tsuji, Numerical evidence of logarithmic regions in channel flow at Reτ=8000,Phys. Rev. Fluids 3, 012602(R) ,2018

[2] Johansson, A. V., Her, J. Y., and Haritonidis, J. H., 1987, “On The Generation of high-amplitude Wall-Pressure Peaks in Turbulent Boundary Layers and Spots”, *J. Fluid Mech.*, Vol. 175, pp. 119-142.

[3] Johansson, A. V., Alfredsson, P. H., and Kim, J., 1991, “Evolution and Dynamics of Shear-Layer Structures in Near-Wall Turbulence”, *J. Fluid Mech.*, Vol. 224, pp. 579-599.

[4] Ali Mehrez, Jimmy Philip, Yoshinobu Yamamoto, and Yoshiyuki Tsuji, Pressure and spanwise velocity fluctuations in turbulent channel flows: Logarithmic behavior of moments and coherent structures, Phys. Rev. Fluids 4, 044601(2019).

[5] J. Jiménez, Coherent structures in wall-bounded turbulence, J. Fluid Mech. 842, 1 (2018).

[6] J. A. Sillero, J. Jiménez, and R. D. Moser, Two-point statistics for turbulent boundary layers and channels at Reynolds numbers up to $\delta^+ \approx 2000$, Phys. Fluids 26, 105109 (2014).